Transient Simulation of a Solar Cavity Receiver for Application in a Low-Latitude Field

Renan de S. Carvalho[1], Gilles Maag[2], John Pye[3], Wojciech Lipiński[3], José R. Simões-Moreira[4] and Celso E. L. Oliveira[2]

[1] University of São Paulo, Institute of Energy and Environment, São Paulo (Brazil)

[2] University of São Paulo, Faculty of Food and Animal Science, Pirassununga (Brazil)

[3] Research School of Electrical, Energy and Materials Engineering, The Australian National University, Canberra (Australia)

[4] University of São Paulo, Polytechnic School, São Paulo (Brazil)

Abstract

Concentrated Solar Power (CSP) has been proposed as a promising renewable alternative to diversify the Brazilian electricity matrix. No CSP plants are operational in Brazil, but R&D projects are under development. In this work, the behavior of a Direct Steam Generation (DSG) receiver based on the SG4 technology to be installed in a 70 kW_e central tower receiver plant, currently under construction in Caiçara do Rio do Vento, RN, Brazil, is simulated via a transient lumped-element numerical model using real meteorological data collected at the installation site. Validation was carried out by comparison of results with a more detailed steady-state model. The results, obtained for a desired steam outlet temperature of 225°C, at a pressure of 14 bar, show convective heat losses to be negligible, compared to reflective and re-radiation losses. The goal of the transient model is to more accurately describe the reactor's behavior during start-up, shutdown, and cloud passage, allowing for insulation dimensioning.

Keywords: concentrated solar power, solar tower, cavity receiver, direct steam generation, transient simulation.

1. Introduction

Historically, the Brazilian electricity mix has largely relied on hydro power. However, in the past years, a need for diversification of the electricity matrix has arisen, given the decreasing relative storage capacity (Oliveira, 2017) of the hydro sector and its consequent increased vulnerability to seasonal drought phenomena (Castro, 2015). While a large expansion of installed photovoltaics and wind power capacity in the Brazilian power grid is under way, the widespread use of those technologies entails the requirement of sufficient grid storage and backup capacity. CSP offers a mitigation of those issues, thanks to its more flexible dispatchability in combination with thermal energy storage. An integration of CSP solutions with thermoelectric power plants in hybrid configurations can increase the capacity factor of the latter. Furthermore, CSP presents the possibility of process heat co-generation, which can lead to cost reductions, e.g. for industrial or agro-industrial consumers.

Given these perspectives, pilot/demonstration endeavors aiming in this direction are under development, such as the SMILE (Solar-hybrid micro-turbine systems for co-generation in agro-industrial electricity and heat production) Project, specifically aiming at hybridization with bio-fuels and co-generation of heat for agro-industrial consumers. In this framework, two pilot solar tower plants are currently under construction, one at the University of São Paulo campus in Pirassununga, São Paulo; and the other in Caiçara do Rio do Vento, Rio Grande do Norte (Maag et al., 2015). In the former, an open volumetric air receiver, coupled to a 70 kW_e Organic Rankine Cycle (ORC) module and a bio-diesel backup burner will be employed, whereas in the latter—the subject of the analysis presented herein—Direct Steam Generation (DSG) cavity receiver powering a 70 kW_e steam engine is foreseen, with a backup boiler fired by eucalyptus pellets. Figure 1 provides artist's views of the two projects. This work aims at numerically predicting and analyzing the transient response of the DSG

doi:10.18086/swc.2019.19.02 Available at http://proceedings.ises.org

solar receiver, under realistic irradiation and temperature conditions based on data collected at the installation site. From this data, as well as on-site observations, a significant amount of single cloud passages, even on clear days, has been noticed, justifying the use of a transient model. Models for solar receivers and receiver-reactors have been proposed in the past (Schunk et al., 2009; Hischier et al., 2010; Maag et al., 2010; Le Roux et al., 2014), including transient ones (Petrasch et al., 2009; Cagnoli et al., 2019; Wheeler et al., 2017, and literature cited therein).

(a) (b)

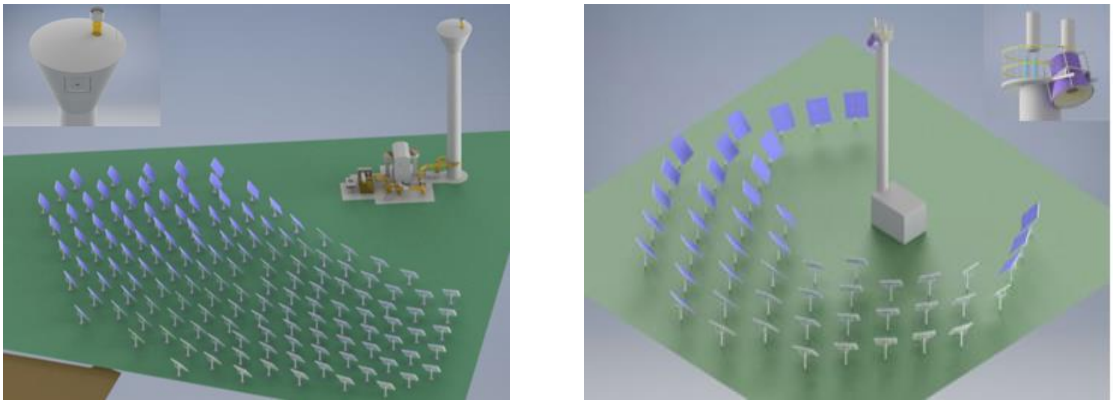

Fig. 1: SMILE Artist's views of power plant projects in Pirassununga (a), and Caiçara do Rio do Vento (b), the latter being the system considered here.

2. Methodology

2.1. Heliostat Field

The considered heliostat field, located at 5.71°S, 36.07° W, is composed of 50 units, each having a square, 9 m² reflective surface, aimed at a focal point positioned atop a 25 m tower. Both the field design and the radiative flux profiles across the focal plane, inclined by 79° with respect to the vertical, in function of the solar vector, have been determined previously. The tower setup is schematically shown in Fig. 2.

2.2. Solar Receiver

Fig. 3 shows the original SG4 cavity receiver (Pye et al., 2017). It consists of a steel tube wound into a coil. By varying the diameter of the windings, two distinct sections are obtained: a receiver plate occupying the peripheral zone of the focal plane, and a receiver cavity with an aperture at the center of the focal region. Those are denominated as "Section 1" ("S1") and "Section 2" ("S2"), respectively. Cold water enters the receiver at the outermost point of Section 1 and proceeds in a spiral movement towards the center, as the diameter of the windings decreases, encountering gradually higher radiative fluxes and heating up. Upon reaching the edge of the cavity aperture, the windings' diameter is kept more constant, leading the fluid into circling the cavity, moving upwards. The cavity configuration allows for the reduction of re-radiation and convection losses from the high-flux, high-temperature region of the receiver.

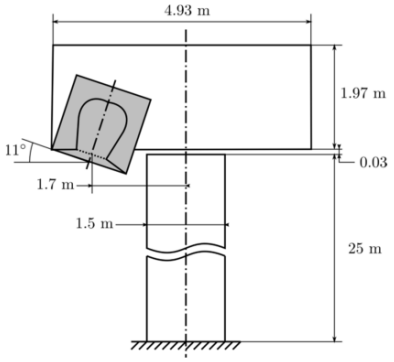

Fig. 2: Schematic of tower geometry and receiver positioning.

Fig. 3: Image of ANU's SG4 cavity receiver (Pye et al., 2017).

An optimization of the system for the specific conditions and design steam outlet conditions (14 bar, 225°C) of the Caiçara plant has been carried out, yielding outer brim and aperture radii R_{brim} = 750 and R_{cavity} = 500 mm, respectively, with the cavity height H_{cavity} being 1000 mm. The average tube outer diameter is 18.9 mm, with a wall thickness of 2.8 mm. Given the inclination of the focal plane due to the tropical location of the site, it will be installed almost vertically, with its axis at 11° with respect to the vertical. The solar field efficiency $\eta_{sf}(\varphi,\theta)$, defined as the fraction of radiative power incident on the receiver versus the radiative power incident on the heliostat field in function of the sun's position, expressed in terms of azimuth and elevation angles φ and θ, was computed prior to this work using the Tonatiuh Monte-Carlo ray-tracing software. For the given geometrical parameters, the design point (sun in Zenith), η_{sf} was calculated to be 0.795, with 58% of the power reaching Section 1 and 42% entering Section 2. At a DNI of 800 W m^{-2}, this amounts to a total incident solar power on the receiver $\dot{Q}_{solar}$ of 286 kW.

For the numerical analysis, the receiver geometry was simplified. For radiative and convective heat transfer purposes, the skirt is assumed to be a diffuse, specular, flat, annular plate, while the cavity is assumed to be a diffuse, specular, flat, cylindrical surface with a diameter equal to that of the aperture. On both surfaces, uniform radiative and convective properties and heat fluxes are assumed. A total absorptivity α of 0.95 and a total emissivity ε of 0.85, typical values for a selective coating, such as Pyromark, are applied. Both sections are insulated by a ceramic foam layer with thermal properties based on those of Thermofelt blanket insulation, that is, a specific heat $c_{p,c}$ of 480 kJ kg^{-1} K^{-1} and a heat conductivity k_c of 0.04 W m^{-1}K^{-1}. For the tube, properties for steel ($c_{p,s}$ = 512.25 kJ kg^{-1} K^{-1}, k_s = 18.8 W m^{-1} K^{-1}) were used. All parameters are assumed to be constant over the considered temperature range. A schematic of the simplified system is shown in Fig. 4. The thickness of the ceramic layer (x_c) is 200 mm and that of the steel layer (x_s) is 18.9 mm.

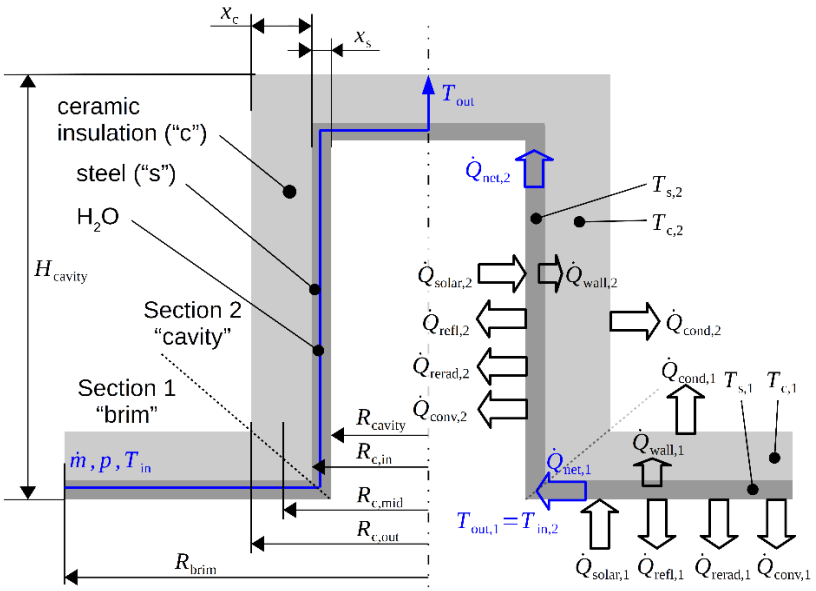

Fig. 4: Simplified reactor geometry, geometric parameters, and variables considered in the transient lumped-element model.

The system is modeled as consisting of four discrete lumped elements, those being the steel tube and the insulation of each section. Fig. 5 shows an infinitesimal receiver element and the considered lump diagram applied to both sections.

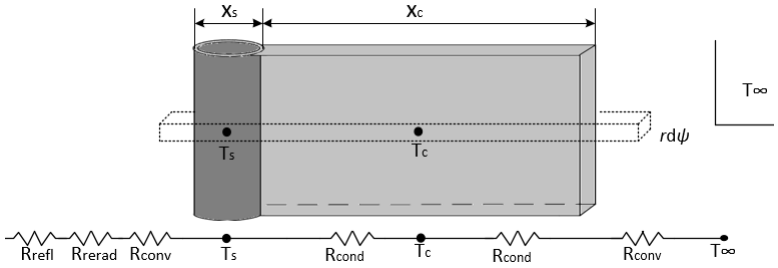

Fig. 5: Infinitesimal element and lump diagram for the considered system.

No heat transfer and fluid dynamic effects within the tube are considered at this stage of the analysis, thus assuming infinitely fast heat transfer through the tube wall and into the fluid, as well as uniform temperature in the tube, justified by its Biot number (Bi = h×L_c/k of 0.001). For each steel and ceramic ("s" and "c") element and section (i = {1,2}), the energy conservation equation is formulated, yielding:

$$m_{\mathrm{s},i} c_{p,\mathrm{s}} \frac{\mathrm{d}T_{\mathrm{steel},i}}{\mathrm{d}t} = \dot{Q}_{\mathrm{solar},i} - \dot{Q}_{\mathrm{refl},i} - \dot{Q}_{\mathrm{rerad},i} - \dot{Q}_{\mathrm{conv},i} - \dot{Q}_{\mathrm{wall},i} - \dot{Q}_{\mathrm{net},i} \quad \text{(eq. 1)}$$

$$m_{\mathrm{c},i} c_{p,\mathrm{c}} \frac{\mathrm{d}T_{\mathrm{ins},i}}{\mathrm{d}t} = \dot{Q}_{\mathrm{wall},i} - \dot{Q}_{\mathrm{cond},i} \quad \text{(eq. 2)}$$

Net power transferred to the water/steam in each section i is:

$$\dot{Q}_{\mathrm{net},i} = \dot{m} \int_{T_{\mathrm{in},i}}^{T_{\mathrm{out},i}} c_{p,\mathrm{H2O}}\,(T_{\mathrm{H2O}})\mathrm{d}T_{\mathrm{H2O}} \quad \text{(eq. 3)}$$

with $T_{\mathrm{in},2} = T_{\mathrm{out},1}$.

Reflection losses are given by $\dot{Q}_{\mathrm{refl},i} = (1-\alpha_i)\dot{Q}_{\mathrm{solar},i}$, where the cavity's apparent absorptivity is $\alpha_2 = \alpha_{\mathrm{app,cavity}} = 0.99$. Re-radiation losses for the two sections are $\dot{Q}_{\mathrm{rerad},1} = A_1 \varepsilon \sigma T_{\mathrm{s},1}$ and $\dot{Q}_{\mathrm{rerad},2} = A_{\mathrm{ap}} \varepsilon_{\mathrm{app,cavity}} \sigma T_{\mathrm{s},2}$, respectively, with $\sigma = 5.6704 \cdot 10^{-8}$ W m^{-2} K^{-4} being the Stefan–Boltzmann constant, $A_1 = \pi\left(R_{\mathrm{brim}}^2 - R_{\mathrm{cavity}}^2\right)$ the Section 1 ("brim") surface area, and $A_{\mathrm{ap}} = \pi R_{\mathrm{cavity}}^2$ the cavity aperture area. The convective heat transfer coefficients ($h_{\mathrm{s},i}$) to compute natural convection losses are calculated by applying a Nusselt correlation for an inclined plate (Incropera et al., 2007) for Section 1 ($\dot{Q}_{\mathrm{conv},1} = A_1 h_{\mathrm{s},1}\left(T_{\mathrm{s},1} - T_\infty\right)$). For the inclined cavity ($\dot{Q}_{\mathrm{conv},2} = A_2 h_{\mathrm{s},2}\left(T_{\mathrm{s},2} - T_\infty\right)$), a different method was considered, proposed by Leibfried and Ortjohann (1995). $A_2 = 2\pi R_{\mathrm{cavity}} H_{\mathrm{cavity}}$ is the inner cavity mantle area. The coefficients for convective heat transfer between the back side of the reactor and ambient ($h_{\mathrm{c},i}$), used in Eqs. (6) and (7), are calculated similarly.

Given the isothermal assumption for the steel coil, conduction through the steel/insulation interface wall is obtained by applying the 1D Fourier equation to the plane Section 1 and cylindrical Section 2:

$$\dot{Q}_{\mathrm{wall},1} = \frac{A_1 k_{\mathrm{c}}\left(T_{\mathrm{s},1} - T_{\mathrm{c},1}\right)}{0.5 x_{\mathrm{c}}} \quad \text{(eq. 4)}$$

$$\dot{Q}_{\mathrm{wall},2} = \frac{2\pi H_{\mathrm{cavity}} k_{\mathrm{c}}\left(T_{\mathrm{s},1} - T_{\mathrm{c},1}\right)}{ln\left(R_{\mathrm{c,mid}}/R_{\mathrm{c,in}}\right)} \quad \text{(eq. 5)}$$

while for conduction losses through the back side of the insulation ($\dot{Q}_{\mathrm{cond},i}$), the electrical circuit analogy is applied:

$$\dot{Q}_{\mathrm{cond},1} = A_1\left(T_{\mathrm{c},1} - T_\infty\right)\left(\frac{0.5x_\mathrm{c}}{k_\mathrm{c}} + \frac{1}{h_{\mathrm{c},1}}\right)^{-1} \quad \text{(eq. 6)}$$

$$\dot{Q}_{\mathrm{cond},2} = 2\pi H_{\mathrm{cavity}}\left(T_{\mathrm{c},2} - T_\infty\right)\left(\frac{ln\left(R_{\mathrm{c,out}}/R_{\mathrm{c,mid}}\right)}{k_\mathrm{c}} + \frac{1}{R_{\mathrm{c,out}}h_{\mathrm{c},2}}\right)^{-1} \quad \text{(eq. 7)}$$

The total heat losses by each section *i* are defined as:

$$\dot{Q}_{\mathrm{loss},,i} = \dot{Q}_{\mathrm{refl},,i} + \dot{Q}_{\mathrm{rerad},,i} + \dot{Q}_{\mathrm{conv},,i} + \dot{Q}_{\mathrm{cond},i} \quad \text{(eq. 8)}$$

Water mass flow rate $\dot{m}$ is the only parameter used to control the outlet steam temperature, keeping it constant at T_{out}. Using Eq. 3, the required flow rate at any time *t* can be determined, via an iterative step in order to ensure $T_{\mathrm{out},1}(t) = T_{\mathrm{in},2}(t)$. A steel temperature $T_\mathrm{s} = T_{\mathrm{out}} + 25°\mathrm{C}$ is chosen as threshold to start water feeding and thus receiver operation. The shutdown criterion is $\dot{Q}_{\mathrm{solar},i} \leqslant \dot{Q}_{\mathrm{losses},i}$, i.e. no solar power for steam generation being available in any of the two sections. Pressure losses in the tube are neglected. Time discretization was carried out by the Forward Euler Method. A Δt of 3 seconds proved sufficient for ensuring numerical stability.

3. Validation

For validation purposes, a comparison of receiver efficiency and injected water mass flow between the transient and a previously formulated steady-state model was carried out at selected days, times, and DNI values. The results are presented in Fig. 6, showing receiver efficiency on January 21st (a) and June 21st (b), 2014, as well as water inlet mass flow on the same days (c and d, respectively) for different DNI sets (1,000, 900, 800, and 500 W m^{-2}), at three different times (solar noon "SN" = 11:35 h, SN + 2 h, and SN + 4 h, UTC-3) of January and June 21st, 2014, considering a pressure of 35 bar, water temperature of 80°C, and steam temperature of 250°C. Comparison of receiver efficiencies and mass flows shows a good agreement for all considered days, DNI and for *t* = SN (Solar Noon, i.e. 11:35 h) and *t* = SN + 2 h, while overestimating efficiency and underestimating mass flow for SN + 4. This is attributed to missing heat transfer and fluid dynamic effects within the tube, not considered yet for the transient model, which may cause discrepancies when operating far from design point.

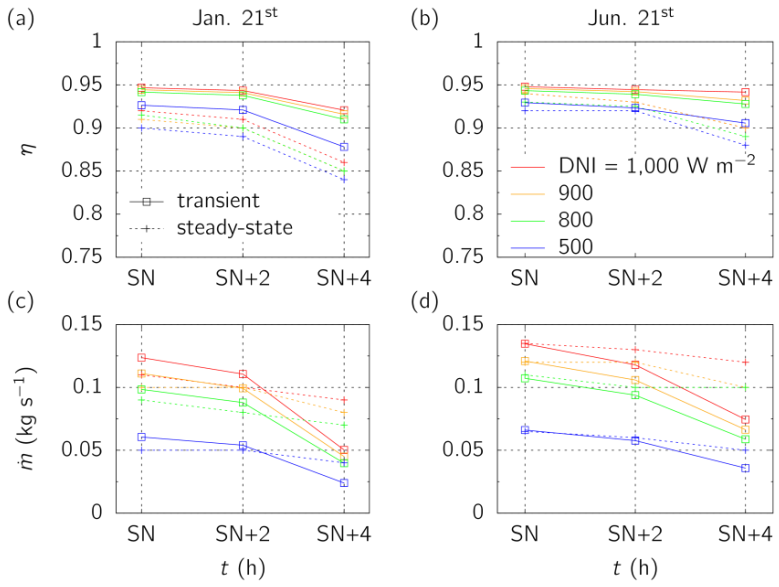

Fig. 6: Comparison of transient results with those of a previously formulated steady-state model at selected times: SN (Solar Noon = 11:35 h). SN + 2 h, and SN + 4 h. The parameters are receiver efficiency on January 21st (a) and June 21st (b), and inlet water mass flow on the same days (c) and (d).

4. Results

From the available meteorological data set, covering 12 months between February 2018 and January 2019, the date of May 5th, 2018, was arbitrarily chosen for the simulations, given the highly-transient behavior of DNI on that specific day. The thermal behavior of the receiver for p = 14 bar, T_{in} = 45°C and T_{out} = 225°C is shown in Fig. 7. The results show a more sensitive behavior of tube temperature on DNI variations, the temperature decreasing *pari passu* with intermittencies. This trend is also found in Section 2, albeit in a smaller scale, which is attributed to the higher thermal inertia and lower re-radiation losses thanks to the cavity effect. As mentioned above, the set threshold for T_s of 250°C can easily be seen.

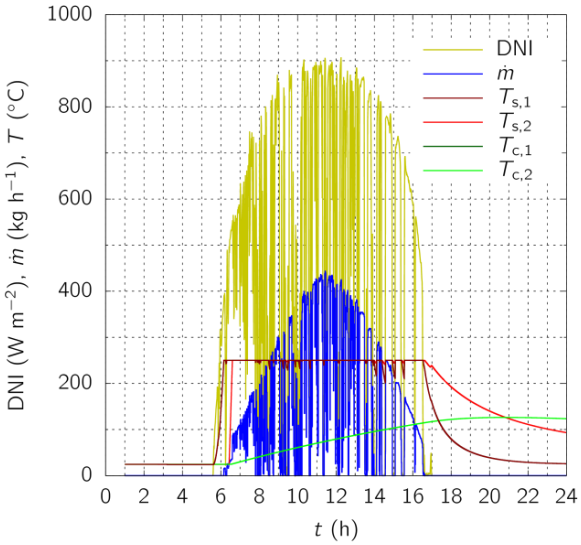

Fig. 7: DNI, temperatures, and H_2O mass flow in function of time on May 5th, 2018.

These steel and ceramic temperature variations due to the transient nature of the DNI can be seen in more detail in Fig. 8, which shows the start-up, cloud passage, and shutdown phase of a typical day (May 5th, 2018). As can be noticed, the operational temperature is reached ca. 0.4 h after sunrise, with Section 1, due to lower mass, taking only half of this time. During a ca. 15 min cloud passage causing a sudden drop of DNI from 800 W m^{-2} to almost zero and back, a small drop (ca. 25°C) is observed in Section 1, whereas the temperature of Section 2 remains practically constant. Finally, during shutdown, a remaining temperature of 90°C for Section 2 is observed at 24:00 h, 7 h after sunset. Due to its thermal mass, the ceramic insulation never reaches steady-state conditions for the given parameters.

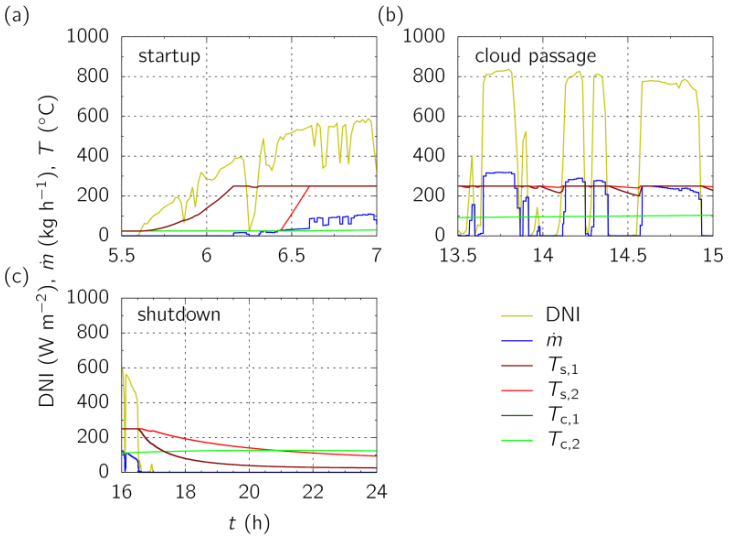

Fig. 8: DNI, inlet water mass flow, and temperature behavior during start-up (a), cloud passage (b), and shutdown (c) on May 5th, 2018.

Figure 9 shows the overall energy balance during the considered 24 h period on May 5th, 2018. Thermal losses

are small in comparison to the receiver net power, re-radiation being the major component (4.7% of total radiative energy incident on the receiver), followed by reflection (3.3%). Losses by conduction through the insulation and convection are negligible (< 1%). Net heat transferred to the fluid over the day is 1,319.2 kWh, or 91.73% of incident solar power, which corresponds to this day's overall receiver efficiency $\eta_{receiver}$.

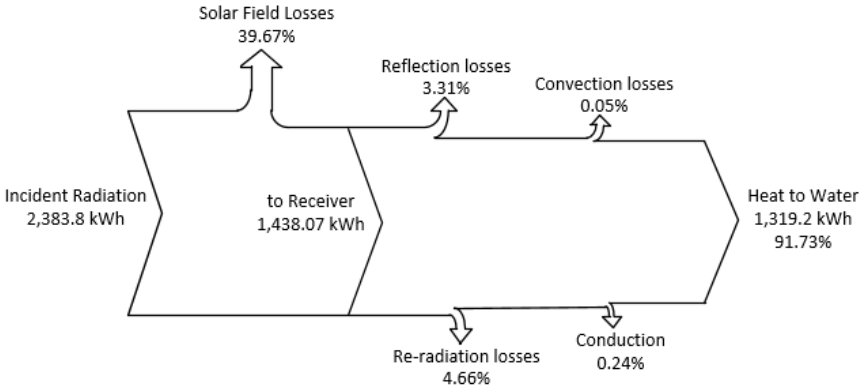

Fig. 9: Sankey diagram with incident radiation, solar field and thermal losses, as well as heat to water energy flow on May 5th, 2018, for both sections.

Those results are in agreement with data from literature, e.g. Ma (1993), who reports that convection losses are low for downward-facing cavity receivers. Hinojosa et al. (2005) also suggested that re-radiation losses are more significant than convective losses for large temperature differences, such as this case, i.e. temperature difference between cavity (steel tubes) and ambient being higher than 200 K.

5. Conclusions

A transient lumped-element numerical model was formulated and validated by comparison to a more detailed, steady-state model, showing good agreement for data points close to the design value. The transient model was applied to predict the thermal performance of a solar cavity receiver based on the SG4 technology that will be installed in a 70 kW_e pilot plant to be built in Caiçara do Rio do Vento, Rio Grande do Norte, Brazil. Real meteorological data collected over 24 h at the installation site during May 5th, 2018, was used as input. The receiver's operational temperature of 250°C is reached within less than 30 min after sunrise. Temperature drop due to a 15 min cloud passage remained below 25°C. Due to its thermal mass, the ceramic insulation never reaches steady-state conditions for the given parameters. The receiver's behavior over a complete 24 h period was simulated. During the simulated period, 1,438.07 kWh of radiative energy reached the reactor. For a desired steam outlet temperature of 225°C and pressure of 14 bar, the results showed predominance of reflection and re-radiation in comparison to convective and conductive losses in both sections. A total steam production of 1,734 kg at above-mentioned conditions is predicted, resulting in an overall reactor efficiency of 91.7%. These results are in accordance with data from the literature, especially regarding convective and re-radiative losses on the inner cavity. A good agreement for regarding the receiver performance, whereas for the water mass flow, especially at 15:35, the results varied substantially, which can be explained by the heat transfer and fluid dynamic effects within the tube not considered at this stage.

6. Acknowledgments

The Authors would like to acknowledge the contributions of R. Gonsales Neto (Solinova Ltda.) and Johannes Hertel (DLR) for information regarding the Caiçara plant. This work was supported by the Brazilian Development Bank (BNDES), through the SMILE (Solar-Hybrid Microturbine Systems for Cogeneration in Agro-Industrial Electricity and Heat Production) Project, and Elektro Eletricidade e Serviços SA through the ANEEL R&D program. R. Carvalho gratefully acknowledges funding of his scholarship by the Coordenação de Aperfeiçoamento de Pessoal de Nível Superior—Brasil (CAPES) —Finance Code 001.

Nomenclature

$\dot{m}$	water mass flow rate, kg h^{-1}
$\dot{Q}$	thermal power, W
T	temperature, °C
t	time, s

Greek letters

α	absorptivity
ε	emissivity
η	efficiency

Subscripts

app	apparent
c	ceramic insulation
cond	conduction losses
conv	convection losses
e	electric
inc	incident radiation from solar field
rad	re-radiation losses
ref	reflection losses
s	steel
sf	solar field

Abbreviations

ANU	The Australian National University
DNI	direct normal irradiance, W m^{-2}
DSG	Direct Steam Generation
USP	University of São Paulo

7. References

Cagnoli, M.; de la Calle, A.; Pye, J.; Savoldi, L.; Zanino, R. A CFD-supported dynamic system-level model of a sodium-cooled billboard-type receiver for central tower CSP applications. **Solar Energy**, v. 177, p.576-594, jan. 2019. Elsevier BV. http://dx.doi.org/10.1016/j.solener.2018.11.031.

Castro, G. M. Avaliação do Valor da Energia Proveniente de Usinas Heliotérmicas Com Armazenamento do Âmbito do Sistema Interligado Nacional. 2015. Universidade Federal do Rio de Janeiro, 2015.

Hinojosa, J. F., Estrada, C. A.; Cabanillas, R. E.; Alvarez, G. Numerical study of transient and steady-state natural convection and surface thermal radiation in a horizontal square open cavity. Numerical Heat Transfer; Part A: Applications, v. 48, n. 2, p. 179–196, 2005.

Incropera, F.P.; Dewitt, D.P.; Bergman, T.L.; Lavine, A.S., 2007. Fundamentals of Heat and Mass Transfer, 7th ed. John Wiley & Sons, Jefferson City.

Leibfried, U., Ortjohann, J., 1995. Convective Heat Loss from Upward and Downward-Facing Cavity Solar Receivers: Measurements and Calculations. J. Sol. Energy Eng. 117, 10. https://doi.org/10.1115/1.2870873.

Ma, R. Y. Wind effects on convective heat loss from a cavity receiver for a parabolic concentrating solar

collector. Sandia Report Contract SAND92-7293.

Maag, G.; Oliveira, K. T.; Oliveira, C. E. L. Hybrid Solar Tower Pilot Plants for Co-Generation of Heat and Power for Brazilian Agro-Industry. In: Proceedings of ISES Solar World Congress 2015, November 2015, Daegu, South Korea.

Oliveira, A.; Salomão, L. A. Setor elétrico brasileiro: Estado e mercado. Rio de Janeiro, RJ: Synergia Editora, 2017. ap. 6. (FGV energia). ISBN 978-85-68483-53-4.

Paitoonsurikarn, S., Lovegrove, K., 2006. A new correlation for predicting the free convection loss from solar dish concentrating receivers. Proc. 44th Conf. Aust. New Zeal. Sol. Energy Soc. (ANZSES), Canberra, Aust. 1–9.

Petrasch, Jörg; Osch, Philippe; Steinfeld, Aldo. Dynamics and control of solar thermochemical reactors. **Chemical Engineering Journal**, v. 145, n. 3, p.362-370, jan. 2009. Elsevier BV. http://dx.doi.org/10.1016/j.cej.2008.07.051.

Pye, J.; Coventry, J.; Venn, F.; Zapata, J.; Abbasi, E.; Asselineau, C.; Burgess, G.; Hughes, G.; Logie, W., 2017 Experimental testing of a high-flux cavity receiver. AIP Conference Proceedings, v. 1850, p. 9